ARTICLE

Structural Analysis of Soft Multicomponent Nanoparticle Clusters

Leonard F. Pease III,[†,‡,§,*] Jeremy I. Feldblyum,[‡,⊥] Silvia H. DePaoli Lacaerda,[‡] Yonglin Liu,[‡] Angela R. Hight Walker,[‡] Rajasekhar Anumolu,[†] Peter B. Yim,[‡] Matthew L. Clarke,[‡] Hyeong Gon Kang,[‡] and Jeeseong Hwang[‡]

[†]Department of Chemical Engineering, University of Utah, Salt Lake City, Utah 84112, United States, [‡]National Institute of Standards and Technology (NIST), Gaithersburg, Maryland 20899, United States, [§]Department of Pharmaceutics & Pharmaceutical Chemistry, University of Utah, Salt Lake City, Utah 84112, United States, and [⊥]Department of Chemistry, University of Maryland, College Park, Maryland 20742, United States

ABSTRACT Quantitative techniques are essential to analyze the structure of soft multicomponent nanobioclusters. Here, we combine electrospray differential mobility analysis (ES-DMA), which rapidly measures the size of the entire cluster, with transmission electron microscopy (TEM), which detects the hard components, to determine the presence and composition of the softer components. Coupling analysis of TEM and ES-DMA derived data requires the creation and use of analytical models to determine the size and number of constituents in nanoparticle complexes from the difference between the two measurements. Previous ES-DMA analyses have been limited to clusters of identical spherical particles. Here, we dramatically extend the ES-DMA analysis framework to accommodate more challenging geometries, including protein corona-coated nanorods, clusters composed of heterogeneously sized nanospheres, and nanobioclusters composed of both nanospheres and nanorods. The latter is critical to determining the number of quantum dots attached to lambda (λ) phage, a key element of a rapid method to detect bacterial pathogens in environmental and clinical samples.

KEYWORDS: composite nanoparticles · electrospray differential mobility analysis · quantum dot · virus · phage · streptavidin

Nanoparticles hold a unique position in nanotechnology[1] because of the ease with which they can be decorated and functionalized to enhance targeting or reactivity, assembled with other nanoparticles into multicomponent nanobioclusters, integrated as detection elements or image contrast agents, and used as vectors to deliver gene and drug therapies.[2−8] This ability to achieve multiple properties with individual nanoparticles or nanoclusters, albeit having a complex mixture of multiple components and soft interfaces, is central to global biological and nanotechnology initiatives.[9−11]

These unique characteristics of nanoparticles and their nanocomplexes facilitate an array of essential advances and challenges for novel applications both *in vivo* and *in vitro*. Examples include advanced cancer treatments, where specifically sized gold nanoparticles are decorated with anticancer moieties (*e.g.*, tumor necrosis factor, TNF) and self-assembled monolayers. These soft, complex nanoparticles are delivered intravenously to leverage the leaky vasculature effect and active targeting, thereby enhancing the efficacy and potentially decreasing the side effects of chemotherapy.[12,13] In contrast, soft multicomponent protein coatings termed coronas rapidly accumulate at the surface of nanoparticles *in vivo*, raising the need for effective biopassivation due to concern about their impact on human health from nanoparticle reactivity and transport (*e.g.*, diffusion) to nontargeted regions.[7,14−19] To enhance the targeting specificity and reduce the risk of potential toxicity, multiple antibody coatings on the surface of quantum dots (QDs) are often administered.[20−22] Antibody-bound nanoparticles are also used regularly for *in vitro* molecular biology to target specific proteins in cells and tissues; dynamic measurements involving protein trafficking have been demonstrated.[23−25] In high-throughput bioassays, quantum dots (QDs) decorate the surface of bacteriophage as a rapid means of detecting harmful bacteria *in vitro*.[25,26] In this case, the bacteriophage targets a specific bacterial strain, while decorated QDs provide a simple and potentially quantitative indicator.

Yet, even as bionanoparticle complexity becomes the norm, it challenges traditional analytical techniques that thrive on simplicity. Indeed, despite the key role of soft complexes, analytical methods to interrogate their presence and properties (*i.e.*, structural (including thickness), mechanical, biological, catalytic, optical, *etc.*) remain insufficient. For instance, while transmission electron microscopy (TEM) produces sharp images of metallic, oxide, and semiconductor nanoparticles, detecting thin organic layers is often fraught with difficulty due to their low contrast, destruction following

*Address correspondence to pease@eng.utah.edu.

Received for review August 22, 2010 and accepted October 22, 2010.

Published online November 4, 2010.
10.1021/nn102106f

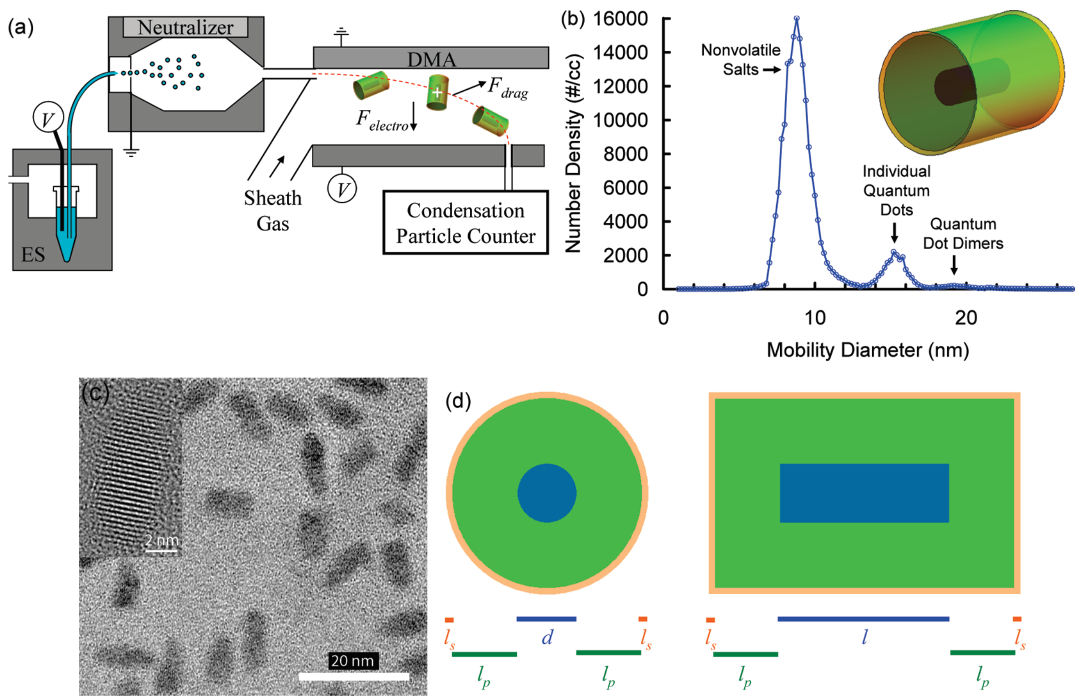

Figure 1. (a) Schematic depicting the major components of the analysis system: electrospray (ES) and neutralizer to set the charge on the dry composite nanoparticle, a differential mobility analyzer (DMA) separating and collecting positively charged particles by their size-to-charge ratio determined trajectory, and a condensation particle counter (CPC) to enumerate them. (b) ES-DMA size distribution showing the gas phase number density *versus* the mobility diameter, d_m, of rod-like streptavidin-coated QDs (maximum of dimer peak at 205 particles/cc). The inset depicts a scale projection of a QD core (dark), streptavidin coating (medium), and thin salt crust (light) remaining from the electrospray process. (c) TEM micrograph of rod-shaped quantum dots. (d) Graphic depicting two orthogonal projections of a streptavidin-coated rod with diameter, d, length, l, salt coating thickness, l_s, and streptavidin coating thickness, l_p.

deposition of thin contrast-enhancing metallic layers, and surface tension-induced aggregation of artifacts on substrates.[10,27,28] Optical techniques (including spectroscopy and scattering) can interrogate the chemical composition and density of organic ligands, but quantitative determination of their thickness or volume is challenging on individual particles (and even more so on clusters) without fluorescent tagging or time-consuming generation of standard curves.[29] Alternatively, the lifetime or blinking rates of QDs may be used to ascertain information regarding the organic coating composition, but this approach remains in its infancy due to lack of comparable measurement techniques and standards for correlating optical properties with the chemical environment of the QD.[30] Despite the challenge, quantitatively characterizing soft, complex nanomaterials is critical to ensuring optical (*e.g.*, photooxidation) and chemical stability during manufacture and storage, correlating pharmacokinetics and toxicity with structure, making rapid bacterial testing quantitative, and enabling regulatory approval, *inter alia*.

Here we use electrospray differential mobility analysis (ES-DMA) with TEM to interrogate critical characteristics of these materials. These two measurements are complementary. ES-DMA measures the overall size of the cluster, including the soft components, while TEM detects the hard components. Both techniques are label-free. As seen in Figure 1a, the DMA sizes positively charged aerosolized particles based on their size-to-charge ratio (analogous to mass spectrometry) because electrical and drag forces compete to set the particle trajectory within the DMA.[31−34] Particles with a select trajectory are individually counted using a condensation particle counter (CPC). Aqueous suspensions of particles are introduced to the DMA by electrospraying them and then reducing the charge on the dried particle to +1, 0, and −1 using a bipolar charge neutralizer.[35] Recent advances in electrospray have improved the reliability of this technique,[25,31−34,36−40] and the resulting charge distribution has been worked out by Wiedensohler.[35] By first charging the particles and then separating them based on their charge-to-size ratio, the ES-DMA separates the soft organic complexes based on size (see Figure 1b). Although historically used to sample environmental aerosols, within the past decade, ES-DMA has been used by several investigators to examine a wide variety of bio/nanoparticles including proteins such as streptavidin; viruses including adenovirus, MS2, lambda (λ) phage, and rhinovirus (HRV2); carbon nanotubes including the length distribution of single-walled carbon nanotubes; and catalysts.[31,33,36,37,40−42]

In a recent paper, the authors developed an analytical model to determine the drag force on close-packed and collinear clusters composed of *identical spheres* and validated the model using clusters of gold nanoparticles.[38] Here, we extend this model to heterogeneously sized spheres and rods with surface-coated organic materials to determine the presence and physical composition of these soft components within nanobiocomplexes. We demonstrate the utility of this approach by first quantifying the amount of streptavidin on protein-coated QDs and subsequently determining the number of QDs attached to the head of a virus, lambda (λ) phage. Both aspects are essential to a recently published strategy to use QD−phage complexes to rapidly detect pathogenic bacterial cells.[25,26] To our knowledge, this is the only drag force model available in the literature to quantify the hard components attached to a soft surface in a statistically reliable manner, overcoming a significant barrier in the analysis of multicomponent nanobioparticles.

RESULTS AND DISCUSSION

The studies reported herein are motivated by the need to overcome a key problem in nanobiotechnology: the lack of characterization tools and methods available to quantify the composition of complex, multiparticle nanobiocomplexes. Our approach integrates ES-DMA with TEM studies. Coupling analysis of TEM and ES-DMA derived data requires the creation and use of analytical models to determine the size and number of constituents in the nanoparticle complex from the difference between the two measurements. Previous ES-DMA drag force models have been limited to clusters of identical spherical particles.[38] Here, we dramatically extend this framework to accommodate more challenging geometries, including thin protein layers on nanorods and nanobioclusters composed of QDs attached to λ phage viruses. We now consider both examples.

The nonspherical structure of commercially available QDs coated with protein is shown in Figure 1. TEM micrographs (Figure 1c) show the streptavidin-coated QDs (Invitrogen, Q10101MP, tethered *via* a short polymer) to be elongated and rod-like.[43,44] The micrographs indicate the cores and shells of the QDs to have an average length of 9.8 ± 2.9 nm, an average diameter of 3.9 ± 0.9 nm, and an average aspect ratio of 2.5 ± 1.1 (uncertainties based on 1σ of multiple measurements, NIST type A uncertainty, and a coverage factor of 2).[45] Although TEM is valuable for establishing the size of the hard central portion of these composite nanoparticles, complementary techniques such as ES-DMA are needed to quantify the softer organic components (*e.g.*, protein and polymer) effectively invisible to TEM. Figure 1b shows the ES-DMA size distribution for the streptavidin-coated quantum rods. There are two primary peaks arising from electrospray droplets that do or do not contain nanoparticles. Less than 1 in 10 droplets emerging from the electrospray contains a QD; the empty evaporating droplets become small spherical salt particles (shape confirmed in TEM)[39] as nonvolatile salts (*e.g.*, borate, phosphate buffered saline, *etc.*)[43] trapped within the droplets precipitate. The first peak centered at d_s = 8.8 ± 1.6 nm (NIST type B uncertainty estimated from the width of the distribution with a coverage factor of 2) represents these particles.[45] The peak centered at 15.2 ± 1.1 nm represents individual QDs. Because nonvolatile salts precipitate onto the surface of the QD as the droplet dries, its actual size is slightly smaller.

To determine the thickness of the organic and salt layers, we turn to the drag force model of Pease *et al.*,[34,38] who showed that the ES-DMA's spherically equivalent aerodynamic or mobility diameter, d_m, may be determined from the nanoparticle's three specific projected areas, A_i, *via*

$$d_m = \left(\frac{\sqrt{\pi}}{6}\sum_{i=1}^{3} A_i^{-1/2}\right)^{-1} \quad (1)$$

This model has previously been used to determine the mobility diameter of identical spherical particles. Here, we extend this framework to nonspherical particles and (below) nanobioclusters composed of multiple heterogeneously sized particles. Each of the projected areas results from a projection normal to a principle axes for the particle system, typically determined by symmetry.[38] For example, the quantum rod with length l and diameter d has a plane of symmetry that bisects the rod, yielding a circular projection, $A_1 = \pi d^2/4$, perpendicular to the central axis of the rod (see Figure 1d, left). The other two projections are identical rectangles, $A_2 = A_3 = dl$ (Figure 1d, right) because of rotational symmetry about the central axis. A bare rod with dimensions indicated by TEM would appear at d_m = 5.5 ± 1.4 nm, far below the 15.2 nm size measured. We model the contribution by the protein and salt layers as cylindrical shells adding an equal (radial) thickness, $l_p + l_s$, to both length and diameter (see Figure 1d), such that $A_1 = \pi(d + 2l_p + 2l_s)^2/4$ and $A_2 = A_3 = (d + 2l_p + 2l_s)(l + 2l_p + 2l_s)$ in eq 1, where l_p represents the thickness of the protein/polymer shell and l_s represents the thickness of the salt shell. Because we know the diameter of the salt particle, we can also construct a volume balance to decouple the contributions of the protein/polymer (an instrument independent material property) and salt (an instrument dependent quantity that varies with ES droplet diameter) as

$$\frac{\pi}{4}(d + 2l_p + 2l_s)^2(l + 2l_p + 2l_s) = \frac{\pi}{6}d_s^3 + \frac{\pi}{4}(d + 2l_p)^2(l + 2l_p) \quad (2)$$

where the first, second, and third terms represent the volume of the salt-encrusted cylinder, the salt sphere (with d_s as its diameter), and a salt-free cylinder, respectively.[37] Solving, we find the thickness of the protein/

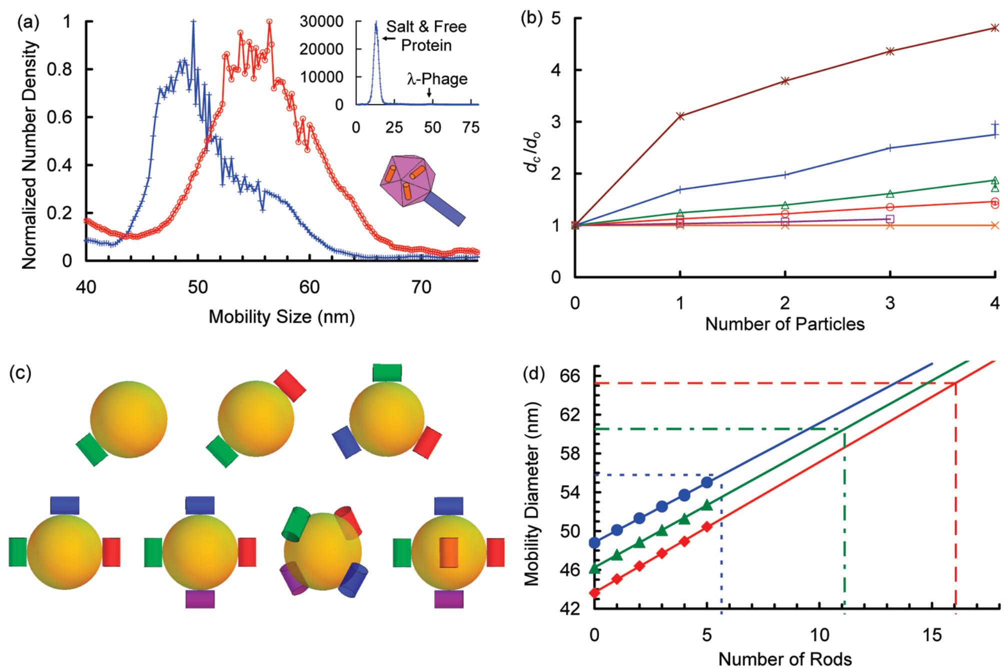

Figure 2. (a) Normalized ES-DMA size distribution of biotinylated λ phage with (○) and without (+) streptavidin-coated quantum rods, normalized on 88.9 and 176.8 phage/cc, respectively. The top inset shows the complete ES-DMA size distribution with units as in Figure 1b, while the bottom inset depicts rod-like QDs attached to an icosahedral virus head. (b) Dimensionless plot of the ratio of the cluster size to the diameter of the central particle, d_c/d_o, *versus* the number of attached spheres for central to external particle diameter ratios, d_o/d_e, of 1/3 (asterisks), 2/3 (+), 1 (triangle), 3/2 (○), 3 (square), 100 (×). (c) Gallery of structures used to estimate the number of streptavidin-coated QDs (right cylinders with lengths and diameters of 18.2 and 11.5 nm, respectively) attached to a biotinylated lambda (λ) phage (spheres with average diameters of 48.8 nm). (d) Predicted mobility diameters, d_m, for the sphere−rod systems shown in panel c *versus* the number of rods in the system, N_r, corresponding to conditions at the mean mobility diameter from panel a (circle, short dash), 1σ out from the means (triangle, alternating dash) and 2σ out from the means (diamond, long dash).

polymer coating and salt shells to be 3.9 and 0.4 nm, respectively. Dividing the volume of the streptavidin layer by the volume of a sphere representing tetrameric streptavidin (6.6 nm diameter as determined by Bacher *et al.*[31]) suggests approximately 12 tetrameric, 24 dimeric, or 48 monomeric molecules per quantum rod to be randomly attached on the surface of the rod, in qualitative agreement with the manufacturer's report of up to 10 tetrameric streptavidins in addition to the polymer. Differentiating the contributions from polymer and protein would require additional stoichiometric or other analysis. In any case, the protein and polymer contribute 94% of the particle's volume (that of the hard core and streptavidin coating are 120 and 1800 nm^3, respectively), indicating the structural importance of this layer (see inset to Figure 1b).

These streptavidin-coated quantum rods were then attached to the surface of λ phage head genetically modified to express biotin.[25] Here, we use a combination of ES-DMA and TEM to determine in detail the number of rods attached, N_r. Figure 2a shows ES-DMA size distributions for biotinylated λ phage with (○) and without (+) streptavidin-coated QDs. For phage without quantum rods, the peak centered at 48.8 nm represents phages with only an icosahedral head, while the shoulder peak centered at 56.1 nm represents a fully intact phage (*i.e.*, with head and tail); most of the tails in both distributions were sheared off in the spin columns (see Supporting Information). The addition of the protein-coated QDs shifts the distribution by 7.0 nm from 48.8 ± 2.6 nm (1σ) to 55.8 ± 4.7 nm. To estimate N_r, the rod-like QDs and icosahedral head of the virus are modeled as right cylinders tangent to a central sphere, respectively, with dimensions that account for the streptavidin coating. TEM images (see Supporting Information) show a propensity for the quantum rods to align parallel to an icosahedral face (~80%) as depicted in the gallery of structures considered in Figure 2c. Each structure is equally weighted in the absence of reason to expect that any structure will predominate.

To demonstrate the validity of this strategy for analysis of heteroclusters, we first consider clusters composed of one central spherical particle of diameter d_o, surrounded by N_s spherical nanoparticles of a second diameter d_e. The diameter of the resulting cluster, d_c, may be obtained *via* eq 1 (see Supporting Information for mathematical analysis). Figure 2b shows that the size of the clusters increases with each additional particle. When $d_o/d_e < 1$, each additional particle adds significantly to the final cluster size before reaching a plateau. However, when $d_o/d_e > 1$, each particle only adds modestly and linearly to the final cluster size. The linearity is crucial because it allows us to linearly extrapolate when the central particle is much larger than the external particles. The latter case applies to the QD−phage complexes.

As seen in Figure 2d, each additional QD adds linearly to the overall mobility diameter. Modestly extrapolating to the arithmetic mean size of the QD−phage complex distribution finds an average of 5.6 QDs per phage—in reasonable agreement with fluorescence microscopy that found 7 ± 3 QDs/phage but in distinct contrast to TEM that indicated 13 ± 4 QDs/phage. Yet, one of the most powerful features of ES-DMA is its ability to provide size distributions based on large populations of nanoparticles. Whereas our TEM result is based on the analysis of 170 of phage−QD complexes, which may or may not represent the true mean value, the ES-DMA measurement is based on a sampled population 3 orders of magnitude larger. Comparing the overlap of the upper wing of the virus size distribution with the lower wing of the cluster size distribution suggests that some viruses may have one or fewer quantum dots attached. Conversely, adding one standard deviation to the mean of the QD−phage complex and subtracting one from the phage distribution finds N_r = 11.1, while adding or subtracting two standard deviations yields N_r = 16.1, respectively. These results indicate that TEM observations alone may lead to overestimates of the *average* number of QDs attached to each phage either because additional QDs enhance the contrast (leading to operator bias in selecting representative particles) or due to accumulation of free rods around the phage in the drying process.[25,27] Centrifuging the phage−QD samples using membrane centrifuge columns in a benchtop centrifuge did not significantly affect the QD/phage ratio measured by TEM.

In summary, the combination of ES-DMA and TEM with analytical models represents a complementary means of interrogating composite nanoparticle conjugates containing organic layers to enable assays requiring quantitative analysis. TEM thrives on measurement of hard materials with complex shapes, while ES-DMA is able to count thousands of nanobioclusters per second, leading to improved statistic confidence in the results relative to the same level of TEM effort with less potential for operator bias. The analytical models reported herein allow for deconvolution of the influence of each distinctly sized component on the total aggregate size using assumptions readily verifiable using TEM. Together they represent a high precision characterization system.

MATERIALS AND METHODS

Electrospray differential mobility analysis (ES-DMA) was used to size three samples. The first contained λ phage at a concentration of 1.0 × 10^{10} phage/mL initially in phosphate buffered saline (PBS). The second sample contained streptavidin-coated quantum rods at a concentration of 1.0 × 10^{13} particles/mL. The third solution contained a biotinylated λ phage (1.0 × 10^{10} phage/mL in PBS prior to biotinylation and mixing) labeled with the streptavidin-coated quantum rods initially at 1.0 × 10^{13} particles/mL. These samples were prepared for ES-DMA by minimizing nonvolatile salts and increasing their concentration as follows. The quantum rod sample was dialyzed for one week into a 2.0 mmol/L ammonium acetate solution at pH 8 with a slide-a-lyzer cartridge (Pierce Biotechnology, IL) having a 10 kDa molecular weight cut off (MWCO). The two phage samples were dialyzed against Nanopure water (Millipore, Billerica, MA) using Spectra/Por Float-A-Lyzer tubing, MWCO 100 000 (Spectrum Laboratories, Rancho Dominguez, CA) for 3 days. The phage samples were further concentrated by 10-fold using spin columns for 16 to 18 min at 3000 rpm, bringing their concentration above the ES-DMA's minimum detection limit. These solutions were transferred to low protein binding 1.5 mL microcentrifuge tubes (Eppendorf, NY), and the phage samples were stored under refrigeration at 4 °C until analysis.

The solutions were electrosprayed (TSI Inc., MN, #3480) to produce a narrow distribution of droplet diameters.[46] The electrospray was operated exclusively in the stable cone-jet flow regime, characterized by visual observation of a sharp cone-shaped meniscus at the tip of a 25 μm inner diameter capillary, although there was some variability in the current within a given sample run (V = 2.25 to 2.36 kV, I = −77 to −95 nA). Immediately downstream of the electrospray, the rapidly evaporating droplets enter a bipolar neutralizer containing a Po-210 ionizing radiation source from which a majority of dried nanoparticles emerge with a charge of +1, 0, or −1. They were then passed into the differential mobility analyzer (DMA) (TSI Inc., MN, #3080), which separates them based on their charge-to-size ratio (or more formally, their mobility). Ones with a select ratio (determined by the electrical and flow fields within the DMA) were sent to a condensation particle counter (CPC) (TSI, MN, USA, #3025A), which measures the concentration of particles entrained in the gas. The sampling flow containing polydispersed aerosols was set to 1.2 L/min, while the nitrogen sheath flow rate was 10 and 30 L/min for phage and other samples, respectively. Because we apply a negative bias to ions within the DMA, only particles that acquire a positive charge are detected. The fraction of particles with a positive charge is size dependent given by Weidensohler.[35] Systematically stepping through electrostatic potentials from 0 to −10 kV, corresponding to 0.2 nm intervals in mobility diameter, builds up a size distribution for positively charged particles. The distribution for all particles regardless of charging efficiency is obtained by dividing the raw counts for positively charged particles at each size by the fraction of positively charged particles at that size. Conversion to size was performed as described in detail elsewhere[34] assuming the particles to be spheres with a Cunningham slip correction factor of $C_c = 1 + Kn[\alpha + \beta \exp(-\gamma/Kn)]$, where $Kn = 2\lambda/d$, d is the particle's diameter, the gas mean free path at room temperature λ = 66 nm, α = 1.257, β = 0.40, and γ = 1.110.[34] This spherically equivalent size is termed the mobility diameter, d_m, and much of the analysis of the ES-DMA size distributions involves extracting structural information from it.[32,38]

Mobility diameters for several structures were calculated in Mathematica (version 6.0, Wolfram Research, Inc., Champaign, IL) using the projected area formalism introduced by Pease *et al.*[34] Please see Supporting Information for further details of the calculation for heterogeneously sized nanospheres. Calculations to predict the mobility diameter of the quantum rod labeled phage assume the icosahedral head to be a 48.8 nm diameter sphere (see Supporting Information for further justification) and the rods to be right cylinders 18.2 nm in length and 11.5 nm in diameter. The rigid cylinders are tangent to the sphere, and the cylinder's axis of symmetry lies parallel to the sphere's nearest tangent plane. Only sphere−cylinder systems with sufficient symmetry to facilitate straightforward identification of the particle system's principle axes were considered. For more complicated geometries, where faces of the rods do not align with the particle's coordinate system, a gravimetric approach was used to determine the projected areas: a structure and its three orthogonal projections were assembled in Mathematica, the projection was printed and cropped, and the relevant areas were determined assuming the paper to be of uniform density and thickness. This latter approach was confirmed to introduce minimal uncertainty when compared to direct geometric calculation.

Samples for transmission electron microscopy (TEM) characterization were prepared by placing several drops of the QD solution onto 300-mesh copper or nickel grids with carbon support film (no. 01753 or no. 01800, Ted Pella). High-resolution TEM (HR-TEM) images were taken from JEOL 2100F field-emission and 2100 LaB6 TEMs at 200 kV. The phage−QD complexes were measured by TEM (Philips 400T) operating at 120 kV equipped with a Soft Imaging System CCD camera (Cantega 2K).

Acknowledgment. The authors would like to express sincere appreciation to Suvajyoti Guha for his assistance with exploratory ES-DMA experiments (not included) and Richard E. Cavicchi for thoughtful discussions. The authors also express appreciation to Michael R. Zachariah of the University of Maryland and Michael J. Tarlov for use of their equipment, facilities, know-how, and shared wisdom. The authors also acknowledge the Maryland NanoCenter and its NispLab, which is partially supported by NSF as a MRSEC Shared Experimental Facility. Reference to commercial equipment, supplies, or software neither implies its endorsement by the National Institute of Standards and Technology (NIST) nor implies it to be necessarily the best suited for this purpose.

Supporting Information Available: Additional details describing the calculations for multiple spheres differing in size and arrangement, TEM micrographs, and ES-DMA peak assignment. This material is available free of charge *via* the Internet at http://pubs.acs.org.

REFERENCES AND NOTES

1. Dreher, K. L. Health and Environmental Impact of Nanotechnology: Toxicological Assessment of Manufactured Nanoparticles. *Toxicol. Sci.* **2004**, *77*, 3–5.
2. Boal, A. K.; Ilhan, F.; DeRouchey, J. E.; Thurn-Albrecht, T.; Russell, T. P.; Rotello, V. M. Self-Assembly of Nanoparticles into Structured Spherical and Network Aggregates. *Nature* **2000**, *404*, 746–748.
3. Claridge, S. A.; Mastroianni, A. J.; Au, Y. B.; Liang, H. W.; Micheel, C. M.; Frechet, J. M. J.; Alivisatos, A. P. Enzymatic Ligation Creates Discrete Multinanoparticle Building Blocks for Self-Assembly. *J. Am. Chem. Soc.* **2008**, *130*, 9598–9605.
4. Ghosh, P.; Han, G.; De, M.; Kim, C. K.; Rotello, V. M. Gold Nanoparticles in Delivery Applications. *Adv. Drug Delivery Rev.* **2008**, *60*, 1307–1315.
5. Loo, C.; Lowery, A.; Halas, N.; West, J.; Drezek, R. Immunotargeted Nanoshells for Integrated Cancer Imaging and Therapy. *Nano Lett.* **2005**, *5*, 709–711.
6. Mamedova, N. N.; Kotov, N. A.; Rogach, A. L.; Studer, J. Albumin−CdTe Nanoparticle Bioconjugates: Preparation, Structure, and Interunit Energy Transfer with Antenna Effect. *Nano Lett.* **2001**, *1*, 281–286.
7. Nel, A.; Xia, T.; Madler, L.; Li, N. Toxic Potential of Materials at the Nanolevel. *Science* **2006**, *311*, 622–627.
8. Rogach, A. L.; Nagesha, D.; Ostrander, J. W.; Giersig, M.; Kotov, N. A. "Raisin Bun"-Type Composite Spheres of Silica and Semiconductor Nanocrystals. *Chem. Mater.* **2000**, *12*, 2676–2685.
9. Guzman, K. A. D.; Taylor, M. R.; Banfield, J. F. Environmental Risks of Nanotechnology: National Nanotechnology Initiative Funding, 2000−2004. *Environ. Sci. Technol.* **2006**, *40*, 1401–1407.
10. Dubertret, B.; Skourides, P.; Norris, D. J.; Noireaux, V.; Brivanlou, A. H.; Libchaber, A. *In Vivo* Imaging of Quantum Dots Encapsulated in Phospholipid Micelles. *Science* **2002**, *298*, 1759–1762.
11. Roco, M. C. International Perspective on Government Nanotechnology Funding in 2005. *J. Nanopart. Res.* **2005**, *7*, 707–712.
12. Toumey, C. Small Differences. *Nat. Nanotechnol.* **2009**, *4*, 275.
13. Paciotti, G. F.; Myer, L.; Weinreich, D.; Goia, D.; Pavel, N.; McLaughlin, R. E.; Tamarkin, L. Colloidal Gold: A Novel Nanoparticle Vector for Tumor Directed Drug Delivery. *Drug Delivery* **2004**, *11*, 169–183.
14. Lundqvist, M.; Stigler, J.; Elia, G.; Lynch, I.; Cedervall, T.; Dawson, K. A. Nanoparticle Size and Surface Properties Determine the Protein Corona with Possible Implications for Biological Impacts. *Proc. Natl. Acad. Sci. U.S.A.* **2008**, *105*, 14265–14270.
15. Cedervall, T.; Lynch, I.; Foy, M.; Berggad, T.; Donnelly, S. C.; Cagney, G.; Linse, S.; Dawson, K. A. Detailed Identification of Plasma Proteins Adsorbed on Copolymer Nanoparticles. *Angew. Chem., Int. Ed.* **2007**, *46*, 5754–5756.
16. Cedervall, T.; Lynch, I.; Lindman, S.; Berggard, T.; Thulin, E.; Nilsson, H.; Dawson, K. A.; Linse, S. Understanding the Nanoparticle−Protein Corona Using Methods To Quantify Exchange Rates and Affinities of Proteins for Nanoparticles. *Proc. Natl. Acad. Sci. U.S.A.* **2007**, *104*, 2050–2055.
17. Hellstrand, E.; Lynch, I.; Andersson, A.; Drakenberg, T.; Dahlback, B.; Dawson, K. A.; Linse, S.; Cedervall, T. Complete High-Density Lipoproteins in Nanoparticle Corona. *FEBS J.* **2009**, *276*, 3372–3381.
18. Lynch, I.; Cedervall, T.; Lundqvist, M.; Cabaleiro-Lago, C.; Linse, S.; Dawson, K. A. The Nanoparticle−Protein Complex as a Biological Entity; A Complex Fluids and Surface Science Challenge for the 21st Century. *Adv. Colloid Interface Sci.* **2007**, *134−35*, 167–174.
19. Balbus, J. M.; Maynard, A. D.; Colvin, V. L.; Castranova, V.; Daston, G. P.; Denison, R. A.; Dreher, K. L.; Goering, P. L.; Goldberg, A. M.; Kulinowski, K. M.; *et al.* Meeting Report: Hazard Assessment for Nanoparticles—Report from an Interdisciplinary Workshop. *Environ. Health Perspect.* **2007**, *115*, 1654–1659.
20. Karwa, A.; Papazoglou, E.; Pourrezaei, K.; Tyagi, S.; Murthy, S. Imaging Biomarkers of Inflammation *In Situ* with Functionalized Quantum Dots in the Dextran Sodium Sulfate (DSS) Model of Mouse Colitis. *Inflammation Res.* **2007**, *56*, 502–510.
21. Jayagopal, A.; Russ, P. K.; Haselton, F. R. Surface Engineering of Quantum Dots for *In Vivo* Vascular Imaging. *Bioconjugate Chem.* **2007**, *18*, 1424–1433.
22. Barat, B.; Sirk, S. J.; McCabe, K. E.; Li, J. Q.; Lepin, E. J.; Remenyi, R.; Koh, A. L.; Olafsen, T.; Gambhir, S. S.; Weiss, S.; *et al.* Cys-Diabody Quantum Dot Conjugates (ImmunoQdots) for Cancer Marker Detection. *Bioconjugate Chem.* **2009**, *20*, 1474–1481.
23. Tokumasu, F.; Fairhurst, R. M.; Ostera, G. R.; Brittain, N. J.; Hwang, J.; Wellems, T. E.; Dvorak, J. A. Band 3 Modifications in Plasmodium Falciparum-Infected AA and CC Erythrocytes Assayed by Autocorrelation Analysis Using Quantum Dots. *J. Cell Sci.* **2005**, *118*, 1091–1098.
24. Wang, S. P.; Mamedova, N.; Kotov, N. A.; Chen, W.; Studer, J. Antigen/Antibody Immunocomplex from CdTe Nanoparticle Bioconjugates. *Nano Lett.* **2002**, *2*, 817–822.
25. Yim, P. B.; Clarke, M. L.; McKinstry, M.; De Paoli Lacerda, S. H.; Pease, L. F., III; Dobrovolskaia, M. A.; Kang, H.; Read, T. D.; Sozhamannan, S.; Hwang, J. Quantitative Characterization of Quantum Dot-Labeled Lambda Phage for *Escherichia coli* Detection. *Biotechnol. Bioeng.* **2009**, *104*, 1059–1067.
26. Edgar, R.; McKinstry, M.; Hwang, J.; Oppenheim, A. B.; Fekete, R. A.; Giulian, G.; Merril, C.; Nagashima, K.; Adhya, S. High-Sensitivity Bacterial Detection Using Biotin-Tagged Phage and Quantum-Dot Nanocomplexes. *Proc. Natl. Acad. Sci. U.S.A.* **2006**, *103*, 4841–4845.
27. Fischer, B. J. Particle Convection in an Evaporating Colloidal Droplet. *Langmuir* **2002**, *18*, 60–67.
28. Taylor, B. J. Analytical Concept-to-Reality Solution for Nanoparticle Array Application Optimization. Ph.D. Thesis, University of Utah: Salt Lake City, 2009.
29. Demers, L. M.; Mirkin, C. A.; Mucic, R. C.; Reynolds, R. A.; Letsinger, R. L.; Elghanian, R.; Viswanadham, G. A Fluorescence-Based Method for Determining the Surface Coverage and Hybridization Efficiency of Thiol-Capped

Oligonucleotides Bound to Gold Thin Films and Nanoparticles. *Anal. Chem.* **2000**, *72*, 5535–5541.
30. Kang, H.; Maye, M. M.; Nykypanchuk, D.; Clarke, M.; Yim, P.; Krogmeier, J.; Briggman, K.; Gang, O.; Hwang, J. Fluorescence Intermittency and Spectral Shifts of Single Bio-conjugated Nanocrystals Studied by Single Molecule Confocal Fluorescence Microscopy and Spectroscopy. *Proc. SPIE* **2007**, *6430*, 1.
31. Bacher, G.; Szymanski, W. W.; Kaufman, S. L.; Zollner, P.; Blaas, D.; Allmaier, G. Charge-Reduced Nano Electrospray Ionization Combined with Differential Mobility Analysis of Peptides, Proteins, Glycoproteins, Noncovalent Protein Complexes and Viruses. *J. Mass Spectrom.* **2001**, *36*, 1038–1052.
32. Pease, L. F.; Elliott, J. T.; Tsai, D. H.; Zachariah, M. R.; Tarlov, M. J. Determination of Protein Aggregation with Differential Mobility Analysis: Application to IgG Antibody. *Biotechnol. Bioeng.* **2008**, *101*, 1214–1222.
33. Pease, L. F., III; Lipin, D. I.; Tsai, D. H.; Zachariah, M. R.; Lua, L. H.; Tarlov, M. J.; Middelberg, A. P. Quantitative Characterization of Virus-like Particles by Asymmetrical Flow Field Flow Fractionation, Electrospray Differential Mobility Analysis, and Transmission Electron Microscopy. *Biotechnol. Bioeng.* **2009**, *102*, 845–855.
34. Pease, L. F.; Tsai, D. H.; Zangmeister, R. A.; Zachariah, M. R.; Tarlov, M. J. Quantifying the Surface Coverage of Conjugate Molecules on Functionalized Nanoparticles. *J. Phys. Chem. C* **2007**, *111*, 17155–17157.
35. Wiedensohler, A. An Approximation of the Bipolar Charge Distribution for Particles in the Submicron Size Range. *J. Aerosol Sci.* **1988**, *19*, 387–389.
36. Lute, S.; Riordan, W.; Pease, L. F., III; Tsai, D. H.; Levy, R.; Haque, M.; Martin, J.; Moroe, I.; Sato, T.; Morgan, M.; *et al.* A Consensus Rating Method for Small Virus-Retentive Filters. I. Method Development. *PDA J. Pharm. Sci. Technol.* **2008**, *62*, 318–333.
37. Pease, L. F.; Tsai, D.-H.; Fagan, J. A.; Bauer, B. J.; Zangmeister, R. A.; Tarlov, M. J.; Zachariah, M. R. Length Distributions of Single Wall Carbon Nanotubes in Aqueous Suspensions Measured by Electrospray-Differential Mobility Analysis. *Small* **2009**, *5*, 2894–2901.
38. Pease, L. F.; Tsai, D.-H.; Hertz, J. L.; Zangmeister, R. A.; Zachariah, M. R.; Tarlov, M. J. Packing and Size Determination of Colloidal Nanoclusters. *Langmuir* **2010**, *26*, 11384–11390.
39. Tsai, D. H.; Pease, L. F.; Zangmeister, R. A.; Tarlov, N. J.; Zachariah, M. R. Aggregation Kinetics of Colloidal Particles Measured by Gas-Phase Differential Mobility Analysis. *Langmuir* **2009**, *25*, 140–146.
40. Hogan, C. J.; Kettleson, E. M.; Ramaswami, B.; Chen, D. R.; Biswas, P. Charge Reduced Electrospray Size Spectrometry of Mega- and Gigadalton Complexes: Whole Viruses and Virus Fragments. *Anal. Chem.* **2006**, *78*, 844–852.
41. Hogan, C. J.; Kettleson, E. M.; Lee, M. H.; Ramaswami, B.; Angenent, L. T.; Biswas, P. Sampling Methodologies and Dosage Assessment Techniques for Submicrometre and Ultrafine Virus Aerosol Particles. *J. Appl. Microbiol.* **2005**, *99*, 1422–1434.
42. Thomas, J. J.; Bothner, B.; Traina, J.; Benner, W. H.; Siuzdak, G. Electrospray Ion Mobility Spectrometry of Intact Viruses. *Spectroscopy* **2004**, *18*, 31–36.
43. http://probes.invitrogen.com/media/pis/mp19000.pdf (downloaded on 11-28-09).
44. Fu, A. H.; Gu, W. W.; Boussert, B.; Koski, K.; Gerion, D.; Manna, L.; Le Gros, M.; Larabell, C. A.; Alivisatos, A. P. Semiconductor Quantum Rods as Single Molecule Fluorescent Biological Labels. *Nano Lett.* **2007**, *7*, 179–182.
45. http://itl.nist.gov/div898/handbook/mpc/section5/mpc5.htm (downloaded on 11-28-09).
46. Loo, J. A. Studying Noncovalent Protein Complexes by Electrospray Ionization Mass Spectrometry. *Mass Spectrom. Rev.* **1997**, *16*, 1–23.